Dynamic Multiple Access Configuration in Intelligent Lifi Attocellular Access Points

HANAA ABUMARSHOUD[ID], **(Member, IEEE), HAMADA ALSHAER**[ID], **(Senior Member, IEEE), AND HARALD HAAS**[ID], **(Fellow, IEEE)**

LiFi R&D Centre, Institute for Digital Communications, School of Engineering, The University of Edinburgh, Edinburgh EH9 3FD, U.K.

Corresponding author: Hamada Alshaer (h.alshaer@ed.ac.uk)

ABSTRACT The exponential growth in the global demand for wireless connectivity calls for efficient and reliable management of the available wireless resources. Light fidelity (LiFi) harnesses the vast untapped wireless transmission resources in the infrared spectrum and visible light spectrum to create ultra-dense wireless networks which support user mobility, multiuser access, and handover. Various multiuser access (MA) protocols have been developed to meet the varying system requirements, including orthogonal multiple access (OMA) and non-orthogonal multiple access (NOMA) schemes. While NOMA, on the one hand, allows for significant enhancement in the achievable data rates, its performance may be severely degraded under particular conditions such as a large number of connected users or users existing in highly symmetrical locations. OMA, on the other hand, provides better link reliability in such scenarios but at the expense of decreased spectral efficiency. Therefore, there is a need to enable a degree of intelligence in the LiFi access point (AP) to facilitate real-time configuration of the MA protocol. To this end, this paper develops a novel cross-layer design framework for dynamic multiple access selections (DMAS) in intelligent LiFi APs. The developed framework runs at LiFi attocell system level and can be configured to cater for various system requirements in terms of sum data rate, average outage probability, and fairness. The obtained results show that DMAS introduces an effective solution for multiuser resource allocation by achieving better satisfaction of the system requirements compared to the static configuration of a single MA scheme.

INDEX TERMS Light fidelity, visible light communications, multiuser access, OMA, NOMA, MAC protocol, LiFi intelligence.

I. INTRODUCTION

The emerging Internet-of-things (IoT) systems and machine type communications (MTC) pose challenging requirements for fifth generation (5G) networks to support high spectrum and medium access efficiency, ultra-low latency communication links and connectivity to a significantly increasing number of mobile devices [1]–[3]. Furthermore, the heterogeneity of wireless devices (e.g. smart-phones, tablets, sensors and machines) offering a variety of services at different levels of performance represents further key challenges in handling the explosive increase in internet data traffic demand [4]–[6]. Visible light communications (VLC) [7]–[9] based light fidelity (LiFi) [1], [10] has

The associate editor coordinating the review of this manuscript and approving it for publication was Mahdi Zareei.

emerged as a promising technology to complement the existing radio frequency (RF) infrastructures [11]. To this end, LiFi access points (APs) are envisioned to be widely deployed to enable high-speed wireless connectivity in various indoor and outdoor environments including airports, stadia, industrial plants, transport systems and underwater submarines, to name a few [12].

A. BACKGROUND AND RELATED WORK

The deployment of enhanced medium access schemes in LiFi attocells is a critical requirement to enable more effective and efficient wireless resource allocation and meet the quality of service (QoS) requirements (e.g., throughput, reliability, coverage, latency, security, and privacy) [13]–[15]. Different multiuser access (MA) schemes have been developed to

meet the demands of various network configurations. Orthogonal multiple access (OMA) schemes, on the one hand, allocate distinct frequency/time/spatial resources to different users, allowing interference-free multi-user access [16]–[18]. On the other hand, non-orthogonal multiple access (NOMA) schemes allow users to share the available frequency/time resources in the same spatial layer. Power-domain NOMA, for example, allocates distinct power levels to different users based on their respective channel conditions in a way that allows each user to recover its own signal [19]–[22], whereas code-domain NOMA employs unique spreading sequences so as to multiplex the users' signals in the code domain, such as the well-known code-division multiple access (CDMA) technique [23], [24]. As a result, NOMA schemes could significantly improve the throughput of LiFi networks and accommodate high-rate services. However, it is impractical to multiplex a high number of users by NOMA as the resulting inter-user interference could lead to severe performance degradation [25], [26]. Furthermore, a hybrid MA scheme that combines OMA and NOMA can better adapt the resource allocation in the LiFi attocellular networks [27]. In this case, the attocell users can be divided into different groups that are multiplexed by an OMA scheme, whereas the users within each group are multiplexed by means of NOMA. It is worth noting that selecting a subset of active users to be multiplexed by power-domain NOMA can reduce the computational complexity and error propagation detection associated with successive interference cancellation (SIC). A Hybrid NOMA precoding scheme with sequential user pairing algorithm was presented in [28] to realize spectral efficiency improvement in a downlink multiple-input-single-output (MISO) scenario. The proposed scheme was shown to achieve significant throughput enhancement and power reduction compared to conventional OMA. The work in [29] proposed rate-splitting multiple access (RSMA) as a general hybrid multiple access scheme for multi-antenna systems. RSMA relies on decoding part of the interference by means of SIC while treating the remaining part of the interference as negligible noise. Results showed that RSMA provides rate and QoS enhancements over NOMA while having a lower computational complexity due to the lower number of SIC layers. It is evident that the decision on MA protocol highly affects the achievable system performance and users' QoS satisfaction. Therefore, it is expected that future wireless networks will integrate hybrid MA techniques. This trend has also been evidenced by the recent application of NOMA to 3GPP-LTE multiuser superposition transmission (MUST) [30]. Particularly, MUST is based on a hybrid MA scheme that combines OFDMA and NOMA based on the channel gain differences between the users.

B. PROBLEM STATEMENT AND MOTIVATION

As discussed earlier, various MA schemes have been investigated in the context of LiFi multiuser scenarios. It is evident that there exists an inevitable trade-off between rate performance, link reliability and users' fairness offered by the

different MA protocols. For example, it was shown in [25] that, while NOMA has the potential to unveil massive capacity gains in LiFi systems, its performance is susceptible to high error rates and reduced link reliability. Furthermore, since the existence of dissimilar channel gains is the basis of successful SIC in NOMA, its application could be restricted by the distinct strong symmetry of the VLC channel. Moreover, the use of power-domain multiplexing and SIC leads to extra computational complexity at the user terminal, which is undesirable for low-power receivers. This problem could be tackled by hybrid OMA/NOMA that allows for less stages on SIC and hence less complexity [31]. This paper works on the premise that a LiFi AP can decide on the best MA strategy to implement for specific users' statistics, i.e., number, locations and QoS requirements of users. As a result, DMAS is expected to be a key feature of LiFi networks in order to support the diverse requirements of different services and applications. We believe that intelligent dynamic real-time MA selection is a particularly critical requirement for future LiFi networks for the following reasons:

1) LiFi APs form small cells with coverage areas of few meters [1], which implies that mobility could result in a rapid change in users' statistics. Thus, a real-time decision-making process is needed to dynamically adapt to the change in the number of connected users.
2) The VLC channel gain mainly relies on the users' spatial locations, and a small change in the user's coordinates may lead to a change in the ordered channel gains of the users, which in turn affect the performance of NOMA.
3) The VLC channel is highly symmetric in nature, which means that two users may exist in completely different positions and yet experience the exact same channel gain. In such scenario, NOMA performance could dramatically degrade and the LiFi AP may need to switch to another MA scheme.
4) Line-of-sight (LOS) is the dominant component of the VLC channel, and multi-path channel gain is negligible in most cases [32]. If a LOS blockage occurs to a particular user, the LiFi AP needs to adapt in real time and asses whether to connect the user via multi-path reflections or to disconnect the user and re-allocate the resources. In both scenarios, real-time decision making process is needed to reconfigure the MA strategy so as to maximize users' satisfaction.

The MA selection process represents the core of intelligence in the LiFi AP, which can run the appropriate alternative to meet the network design requirements. The research problem of MA configuration in LiFi APs can be decomposed into three main sub-problems: i) obtaining real-time information and QoS requirements of the LiFi downlink system, ii) developing mathematical and computational tools to support the subjective evaluation of a finite number of alternative MA schemes under specific performance criteria, and iii) employing an appropriate multi-criteria decision aid

mechanism to choose among the configured MA schemes. Motivated by the above, we propose a solution for intelligent and self-configurable LiFi network access. In the proposed framework, the attocell AP can autonomously decide on the MA strategy so as to efficiently utilize the available resources to support the different requirements of the network users. To the best of the authors' knowledge, the problem of dynamic MA selection has not been investigated in related literature. A detailed outline of the contribution of this work is provided in the following subsection.

C. CONTRIBUTION

The developed DMAS scheme is envisioned to enable LiFi APs to support resource-efficient multiple user access and service provisioning operations in any device or environment. DMAS enables a LiFi AP to autonomously decide on the MA mode so as to efficiently support the different requirements of LiFi network operations and the network users. The contributions of this paper can be described as four-fold:

1) DMAS is proposed to enable adaptive configuration of the available supported MA modes, i.e., OMA, NOMA and hybrid OMA/NOMA.
2) The decision-making process in DMAS is based on different attributes, namely: sum rate, outage probability and Jain's fairness index. Closed-form expressions for each of the design attributes are developed for the different MA modes under consideration.
3) The proposed DMAS can be dynamically adapted by allocating different weights to the different design attributes so as to support diverse LiFi-based services and applications
4) A simulation environment is developed to investigate the performance of the considered MA schemes and the proposed DMAS. The presented simulation results demonstrate that DMAS provides better satisfaction of the system requirements compared to a static configuration of a single MA scheme.

D. STRUCTURE

The rest of this paper is structured as follows. Section II describes the LiFi downlink framework, including the VLC channel model and DCO-OFDM transmission. The different MA schemes are presented in Section III, while Section IV describes the proposed DMAS scheme and its underlying process. The evaluation of different attributes characterizing the MA schemes under consideration are presented in Section V. Section VI provides simulation results and related discussions. Finally, closing remarks are drawn in Section VII.

II. LIFI DOWNLINK FRAMEWORK

In this section, we describe the framework of the downlink LiFi network adopted in this study. We consider an attocell AP that simultaneously serves multiple users located under its coverage area. The uplink connection could be possibly realized by means of RF or infra-red (IR), and is out of the scope of this study [33]–[35]. As a result, it is assumed that there is no interference between the uplink and the downlink transmissions. Furthermore, it is assumed that the AP users do not exhibit interference from neighbouring LiFi APs. It is noted that this is a common assumption in related literature validated by the fact that light signals do not penetrate through walls, which enables having an interference-free LiFi attocell built into a room [32], [36]. Furthermore, the AP is assumed to have channel state information (CSI) of all users in its coverage area, which is a common assumption in related literature [27], [37], [38]. We consider that the attocell circular coverage area is divided into a cell centre area and a cell edge area as shown in Fig. 1. The cell centre is formed by a circle centred at the AP with radius r_A, whereas the cell edge comprises the ring bounded by r_A and r_B. Accordingly, the attocell users are classified into cell centre users, i.e., $U_A = \{U_{A_i}\}_{i=1}^{N_A}$, and cell edge users, i.e., $U_B = \{U_{B_j}\}_{j=1}^{N_B}$. To facilitate multi-user access, the attocell AP dynamically decides on the MA scheme such that the available system resources are best utilized to meet specific system requirements. The proposed DMAS runs on the LiFi AP which collects users' information, i.e., CSI and QoS requirements, and evaluates the performance of the different configured MA scheme, namely: OMA, NOMA and hybrid OMA/NOMA. It is noted that OMA in the proposed framework is implemented by means of orthogonal frequency division multiple access (OFDMA), while NOMA refers to power-domain NOMA. Also, all transmissions are based on direct current biased optical orthogonal frequency division multiplexing (DCO-OFDM) [39], [40]. It is noted, however, that the present analysis can be easily extended to different optical OFDM schemes. Furthermore, in order to enable the selection process, the proposed DMAS scheme should have a flexible frame structure so that the time and frequency resources are partitioned into different blocks that are freely available for different services and users.

A. VLC CHANNEL MODEL

The VLC channel is influenced by the characteristics of front-end devices as well as the free-space transmission. Therefore, we model the VLC channel gain at user k for subcarrier n as follows:

$$H_k(n) = H_k^{\text{fe}}(n) H_k^{\text{fs}}(n), \tag{1}$$

where $H_k^{\text{fe}}(n)$ and $H_k^{\text{fs}}(n)$ represent the frequency response due to front-end devices filtering and free-space optical channel, respectively. The low-pass filtering response of front-end devices can be approximated as:

$$H_k^{\text{fe}}(n) = \exp(-\frac{nF_s}{N_{\text{FFT}}F_{\text{fe}}}), \tag{2}$$

where $n = 1, 2, \ldots, N_{\text{FFT}}/2 - 1$, N_{FFT} is the total number of subcarriers, F_s is the sampling frequency and F_{fe} controls the frequency characteristics of the front-end device [32].
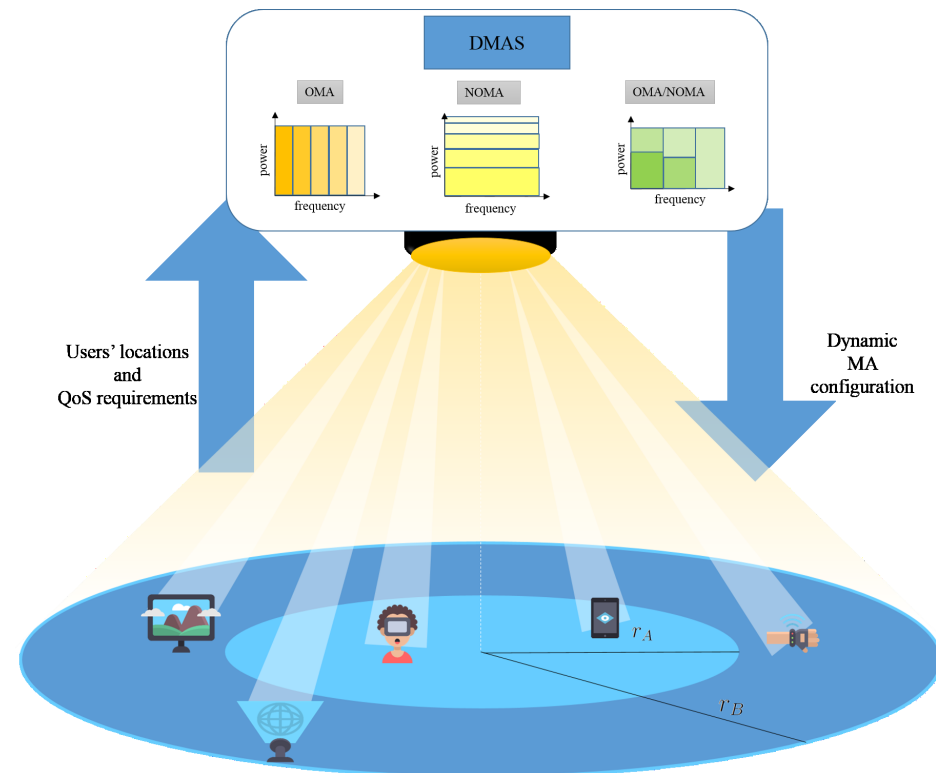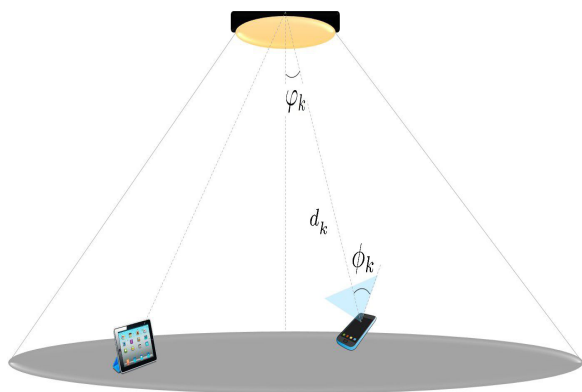
FIGURE 1. LiFi downlink framework.

FIGURE 2. VLC channel model.

The free-space optical channel response can be represented as the LOS channel from the attocell AP to the k-th user. It was shown in [32], that the majority of the attocell users experience negligible multi-path reflections, resulting in a dominant LOS channel component above 80% for the majority of the users. As a result, we can say that $|H_k^{\text{fs}}(n)| = H_k^{\text{LOS}}$, which can be calculated from Fig. 2 as:

$$H_k^{\text{LOS}} = \begin{cases} \dfrac{A_k}{d_k^2} R_o(\varphi_k) T_s(\phi_k) g(\phi_k) \cos(\phi_k), & 0 \le \phi_k \le \phi_c \\ 0, & \phi_k > \phi_c \end{cases}$$

$$(3)$$

where A_k is the receiver photo-detector (PD) area, d_k represents the distance between the AP and the k-th user, φ_k is the angle of emergence with respect to the transmitter axis, ϕ_k is the angle of incidence with respect to the receiver axis, ϕ_c is the field of view (FOV) of the receiving PD, $T_s(\phi_k)$ is the gain of optical filter and $g(\phi_k)$ is the gain of the optical concentrator, which is expressed as:

$$g(\phi_k) = \begin{cases} \dfrac{n^2}{\sin^2(\phi_c)}, & 0 \le \phi_k \le \phi_c \\ 0, & \phi_k > \phi_c \end{cases} \qquad (4)$$

where n denotes the corresponding refractive index. Moreover, $R_o(\varphi_k)$ in (3) is the Lambertian radiant intensity of the LED, which is calculated as:

$$R_o(\varphi_k) = \frac{(m+1)}{2\pi} \cos^m(\varphi_k), \qquad (5)$$

where m is the order of Lambertian emission, expressed as:

$$m = \frac{-\ln(2)}{\ln(\cos(\varphi_{1/2}))}, \qquad (6)$$

with $\varphi_{1/2}$ denoting the LED semi-angle at half power. Assuming a fixed FOV, the channel gain in (3) can be expressed as a function of the distance between the transmitting LED and the receiving PD, which is given as:
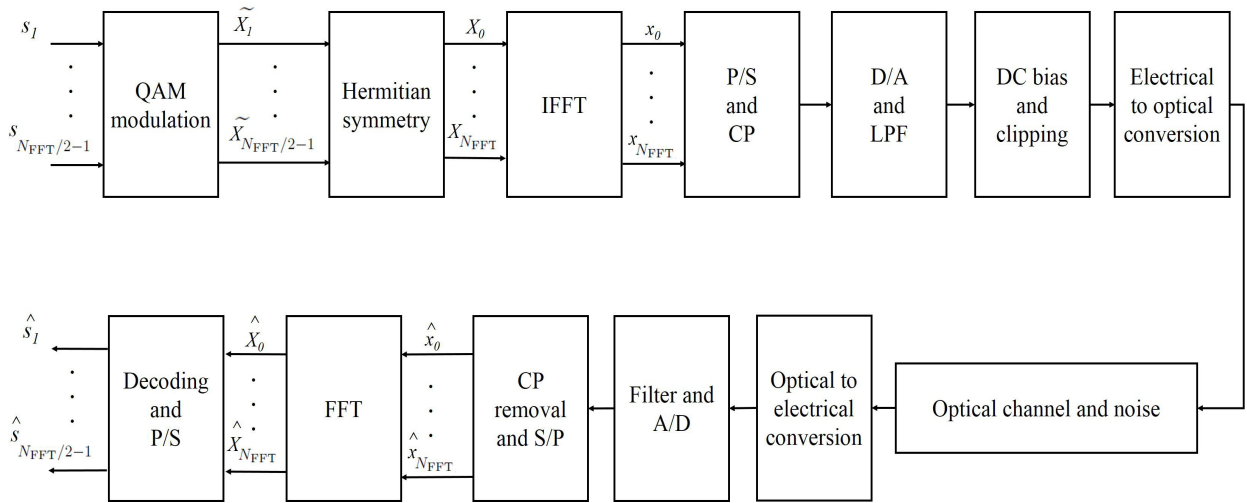
$$H_k^{\text{LOS}} = \zeta \frac{1}{d_k^{m+3}}, \qquad (7)$$

FIGURE 3. Block diagram of DCO-OFDM transceiver.

where $\zeta = \frac{(m+1)}{2\pi} A_k T_s(\phi) g(\phi) z^{m+1}$. Furthermore, the k-th user's location is represented by the polar coordinates (r_k, ψ_k). Thus, given that $d_k = \sqrt{(r_k^2 + z^2)}$, we can write:

$$H_k^{\text{LOS}} = \zeta \frac{1}{(r_k^2 + z^2)^{\frac{m+3}{2}}}, \tag{8}$$

with z being the vertical distance from the PD to the AP level, which is assumed to be fixed.

B. DCO-OFDM TRANSMISSION

The block diagram of a DCO-OFDM transceiver is shown in Fig. 3. In order to obtain a real-valued signal, only a total of $(N_{\text{FFT}} - 2)/2$ effective subcarriers out of N_{FFT} available subcarriers are utilized for data transmission. The parallel bit streams, denoted by $\{s_n\}_{n=1}^{N_{\text{FFT}}/2-1}$ are mapped onto M-order quadrature amplitude modulation (QAM) symbols to generate the complex valued signals $\{\tilde{X}_n\}_{n=1}^{N_{\text{FFT}}/2-1}$. The OFDM frame is then generated by expanding $\{\tilde{X}_n\}_{n=1}^{N_{\text{FFT}}/2-1}$ to $\{X_n\}_{n=0}^{N_{\text{FFT}}}$ according to the Hermitian symmetry mapping, i.e, $X_n = \tilde{X}_n$ for $n = 1, 2, \ldots, \frac{N_{\text{FFT}}}{2} - 1$, $X_n = \tilde{X}_n^*$ for $n = \frac{N_{\text{FFT}}}{2} + 1, \frac{N_{\text{FFT}}}{2} + 2, \ldots, N_{\text{FFT}}$, and $X_0 = X_{\frac{N_{\text{FFT}}}{2}} = 0$. It was shown in [41] that a total subcarrier number as small as 64 is considered sufficient to ensure Gaussianity. Consequently, the resulting OFDM signal is assumed to follow a Gaussian distribution according to the central limit theorem. Next, a cyclic-prefix (CP) is added to the OFDM frame and the time domain signal is clipped, amplified and DC biased in order to ensure the signal is positive. At the user terminal, the received time-domain signal at the k-th user PD can be written as:

$$y_k(t)$$
$$= \eta_{\text{PD}} P_{\text{elec}} \left(x_k(t) + \sum_{i \neq k} x_i(t) \right) \circledast h_k(t) + n_{\text{Rx}}(t), \tag{9}$$

where P_{elec} is the LED electrical power, η_{PD} is the the PD responsivity, $h_k(t)$ denotes the channel gain from the AP to the k-th user. Also $n_{\text{Rx}}(t)$ denotes the receiver noise. The resulting signal is then fed into fast Fourier transform (FFT) to reconstruct the frequency-domain received signal sample for the k-th user at subcarrier n as follows:

$$Y_k(n)$$
$$= \eta_{\text{PD}} P_{\text{elec}} H_k(n) \left(X_k(n) + \sum_{i \neq k} X_i(n) \right) + N_{\text{Rx}}(n), \tag{10}$$

where $H_k(n)$ is the frequency response of the VLC channel of the k-th user at subcarrier n.

C. SINR CHARACTERIZATION

The received signal-to-interference-and-noise ratio (SINR) at the user terminals is an important factor in determining the service quality, and will be used to evaluate various performance metrics in this study. Since we assume that the attocell users do not receive interference from neighbouring LiFi attocells, the interference term in the SINR here refers to interference from signals of other users in the same attocell. The received SINR at the k-th user at subcarrier n can be calculated as:

$$\gamma_k(n) = \frac{\eta_{\text{PD}}^2 P_{\text{elec}}^2 P_k^2 H_k^2(n)}{\underbrace{\eta_{\text{PD}}^2 P_{\text{elec}}^2 H_k^2(n) \left(\sum_{i \neq k} \Pi_{ik}(n) P_i^2 \right)}_{\text{interference}} + \underbrace{\sigma_{\text{Rx}}^2}_{\text{Rx noise}}}, \tag{11}$$

where P_k denotes the power allocated to the k-th user signal, and the function $\Pi_{ik}(n)$ is defined as:

$$\Pi_{ik}(n) = \begin{cases} 1 & X_k(n) \neq 0 \\ 0 & X_k(n) = 0. \end{cases} \tag{12}$$

Hence, the SINR reduces to signal-to-noise ratio (SNR) when a subcarrier, n, is dedicated to a certain user. Using (2) and (8), the SINR expression can be written as:

$$
\begin{aligned}
&\gamma_k(n) \\
&= \left(\frac{\sum_{i \neq k} \Pi_{ik}(n) P_i^2}{P_k^2} + \frac{\sigma_{\mathrm{Rx}}^2 (r_k^2 + z^2)^{m+3}}{\exp(-\frac{nF_s}{N_{\mathrm{FFT}}F_{\mathrm{fe}}}) \zeta^2 \eta_{\mathrm{PD}}^2 P_{\mathrm{elec}}^2 P_k^2} \right)^{-1}.
\end{aligned}
$$

(13)

It can be inferred from (13) that the statistics of the SINR can be easily calculated knowing r_k, i.e., the horizontal distance between the AP and the k-th user, as well as the adopted power allocation strategy.

III. MULTIPLE ACCESS MODES
In this section, we discuss the three MA modes considered in the adopted framework, namely: OMA, NOMA and hybrid OMA/NOMA. The LiFi AP autonomously chooses one of the three modes based on the system parameters using DMAS, as will be discussed later.

A. OMA MODE
In the OMA mode, the attocell AP multiplexes users by means of OFDMA, based on the DCO-OFDM transmission model described in Section II-B. Assuming that all users have equal average access probability (AAP), N_k effective subcarriers are allocated to each user such that $\bar{N}_1 = \ldots = \bar{N}_K = (N_{\mathrm{FFT}} - 2)/2K$, where $\bar{N}_k$ is the expected value of N_k. The time-domain signals after the IFFT operation are transmitted with full power, since each subcarrier is dedicated to a certain user. As a result, there is no interference affecting the k-th user signal at subcarrier, n, and the corresponding received SINR in (13) reduces to SNR as follows:

$$
\gamma_k^{\mathrm{OMA}}(n) = \frac{\exp(-\frac{nF_s}{N_{\mathrm{FFT}}F_{\mathrm{fe}}}) \zeta^2 \eta_{\mathrm{PD}}^2 P_{\mathrm{elec}}^2}{\sigma_{\mathrm{Rx}}^2 (r_k^2 + z^2)^{m+3}}
$$

(14)

B. NOMA MODE
In the NOMA mode, DCO-OFDM is combined with power-domain NOMA so as to multiplex the attocell users in the power domain. To this end, each user's signal utilizes the whole $(N_{\mathrm{FFT}} - 2)/2$ effective subcarriers. The time-domain signals for all K users are superposed in the power domain, where the k-th user signal is multiplied by a power allocation coefficient, P_k. Thus, the overall combined signal can be written as:

$$
\tilde{x} = \sum_{k=1}^{K} P_k \tilde{x}_k.
$$

(15)

In order to satisfy the total transmit power constraint, the power allocation coefficients need to satisfy $\sum_{k=1}^{K} P_k^2 = 1$. To this end, the attocell AP allocates higher power allocation coefficients to users with lower channel gains so as to facilitate SIC at the receiving terminals. Assuming that the users $U_1, U_2 \ldots, U_K$ are sorted in an ascending order

according to their channel gains, i.e. $h_1 \leq h_2 \leq \cdots \leq h_K$, the attocell AP allocates the power allocation coefficients such that $P_1 \geq P_2 \geq \cdots \geq P_K$. As a result, on the one hand, the user with the highest allocated power, i.e., U_1 directly decodes its signal regarding the interference from other signals as negligible noise. On the other hand, users with a higher decoding order, i.e., $U_2, \ldots, U_K$ need to successfully decode and subtract the signals of all other users with a lower decoding order before decoding their own signals. We assume that the attocell AP allocates power coefficients using fixed power allocation (FPA), which is a simple strategy adopted in various related papers [20], [21], [25], [27]. In FPA, the power coefficient associated with the k-th sorted user is set to $P_k = \alpha P_{k-1}$ with α denoting the power allocation factor $(0 < \alpha < 1)$. Consequently, the SINR at the k-th user at subcarrier n in NOMA can be written as:

$$
\begin{aligned}
&\gamma_k^{\mathrm{NOMA}}(n) \\
&= \left(\frac{\sum_{i=k+1}^{K} P_i^2}{P_k^2} + \frac{\sigma_{\mathrm{Rx}}^2 (r_k^2 + z^2)^{m+3}}{\exp(-\frac{nF_s}{N_{\mathrm{FFT}}F_{\mathrm{fe}}}) \zeta^2 \eta_{\mathrm{PD}}^2 P_{\mathrm{elec}}^2 P_k^2} \right)^{-1}.
\end{aligned}
$$

(16)

It is assumed that the signals of users with a lower decoding order are perfectly cancelled during SIC process. Thus, the interference term in (16) accounts only for the interference from the signals of users with a higher decoding order, i.e., signals with low power compared to the desired signal, which can be treated as noise.

C. HYBRID OMA/NOMA MODE
The hybrid OMA/NOMA mode combines NOMA and OMA to find a better trade-off between throughput and reliability [42], [43]. To facilitate this, the entity of users is divided into pairs and each pair is multiplexed in the power domain by means of NOMA. Furthermore, the signals of the different pairs are multiplexed in the frequency domain by allocating distinct subcarriers to each pair's signal. It was shown in [27] that NOMA achieves the maximum sum rate by pairing the two users with the most distinctive channel conditions. To this end, we assume that the Attocell AP multiplexes the signals of pair i with U_{i_1} and $U{i_2}$ only if $h_{i_1} << h_{i_2}$. Thus, a NOMA pair in the hybrid mode consists of a cell edge user paired with a cell centre user, i.e., $r_A \leq r_{i_1} \leq r_B$ and $r_{i_2} \leq r_A$. As a result, the information-bearing time-domain signal transmitted to the i-th pair is $P_{i_1} x_{i_1} + P_{i_2} x_{i_2}$ such that $P_{i_2} = \alpha P_{i_1}$ and $P_{i_1} + P_{i_2} = 1$. The unpaired users, if any, are then allocated distinct subcarriers. It is assumed that each paired and unpaired user have the same AAP, i.e., $\{\bar{N}_i\}_{i=1}^{N_{\mathrm{pairs}}} = \{\bar{N}_j\}_{j=1}^{N_{\mathrm{unpaired}}} = \frac{(N_{\mathrm{FFT}}-2)/2}{N_{\mathrm{pairs}}+N_{\mathrm{unpaired}}}$, where N_{pairs} and N_{unpaired} denote the number of pairs and the number of unpaired users, respectively. Also, N_i is the number of effective subcarriers allocated to pair i while N_j denotes the number of subcarriers allocated to each unpaired user, U_j. Consequently, the unpaired users do not exhibit any multi-user interference and their respective

SNR can be expressed as:

$$\gamma_{k_{\text{unpaired}}}^{\text{Hybrid}}(n) = \frac{\exp(-\frac{nF_s}{N_{\text{FFT}}F_{\text{fe}}})\zeta^2\eta_{\text{PD}}^2 P_{\text{LED}}^2}{\sigma_{\text{Rx}}^2(r_k^2 + z^2)^{m+3}}, \quad (17)$$

while the SINR for the users in ith pair can be written as:

$$\gamma_{i_{\text{pair}}}^{\text{Hybrid}}(n) =$$

$$\begin{cases} \dfrac{\exp(-\dfrac{nF_s}{N_{\text{FFT}}F_{\text{fe}}})\eta_{\text{PD}}^2 P_{\text{LED}}^2 \zeta^2 \eta_{\text{PD}}^2 P_{\text{LED}}^2 P_{i_2}^2}{(r_{i_2}^2 + z^2)^{m+3}\sigma_{\text{Rx}}^2} \\ \qquad\qquad \text{for } U_{i_2} \\ \left(\dfrac{P_{i_2}^2}{P_{i_1}^2} + \dfrac{\sigma_{\text{Rx}}^2(r_{i_1}^2 + z^2)^{m+3}}{\exp(-\dfrac{nF_s}{N_{\text{FFT}}F_{\text{fe}}})\zeta^2 \eta_{\text{PD}}^2 P_{\text{elec}}^2 P_{i_1}^2} \right)^{-1} \\ \qquad\qquad \text{for } U_{i_1}. \end{cases}$$

$$(18)$$

IV. DYNAMIC MA SELECTION (DMAS) SCHEME

The developed DMAS runs based on the technique for order of preference by similarity to ideal solution (TOPSIS) [44]. It evaluates a number of common design parameters for the considered MA schemes. It then computes the quantitative values of considered attributes to determine the positive ideal solution (PIS) and the negative ideal solution (NIS). The PIS maximizes the benefit criteria and minimizes the cost criteria, whereas the NIS maximizes the cost criteria and minimizes the benefit criteria. Next, a decision is made to choose a MA scheme that simultaneously has the shortest distance from the PIS and the farthest distance from the NIS. To this end, the proposed DMAS uses a monitor and computing module, which continuously measures the values of considered system parameters and QoS indicators. It uses the values of these parameters to enable the LiFi AP to select and configure the MA scheme. The following subsections, introduce the DMAS alternatives, attributes and decision-making mechanism.

A. DMAS ALTERNATIVES

In the proposed framework, multi-user access in the attocell can alternate among the three MA modes discussed in the previous section, hence, the possible decision alternatives are:
- OMA mode,
- NOMA mode,
- Hybrid OMA/NOMA mode.

B. DMAS ATTRIBUTES

For the MA selection problem, the following set of attributes are considered in the decision making process:
- **Sum rate, R_{sum}**: which is defined as the total achievable data rate of the attocell constituting of the sum of the data rates of all its users.
- **Outage probability, P_{out}**: which is defined as the average of outage probabilities of all attocell users. An outage occurs for a user if its received SINR value is less than the required SINR threshold of this user.

- **User fairness, $\mathcal{F}$**: which quantifies the notion of resource allocation fairness among the attocell users, and is evaluated by means of Jain's fairness index.

In order to evaluate these attributes, the proposed DMAS requires the knowledge of the location of each attocell user so as to determine the received SINR levels based on (14), (16), (17) and (18). MA scheme selection can then be performed to meet the QoS requirements for cell-centre and cell-edge users.

C. DMAS MECHANISM

The stepwise procedure of DMAS is described below:
- Step 1: collect the input parameters (users' coordinates and QoS requirements).
- Step 2: construct the evaluation matrix, $\mathbf{D} = (\delta_{ij})_{3\times 3}$, with the three MA alternatives and their respective attributes' values as follows:

$$\begin{bmatrix} \delta_{11} & \delta_{12} & \delta_{13} \\ \delta_{21} & \delta_{22} & \delta_{23} \\ \delta_{31} & \delta_{32} & \delta_{33} \end{bmatrix} = \begin{bmatrix} R_{\text{sum}}^{\text{OMA}} & P_{\text{out}}^{\text{OMA}} & \mathcal{F}^{\text{OMA}} \\ R_{\text{sum}}^{\text{NOMA}} & P_{\text{out}}^{\text{NOMA}} & \mathcal{F}^{\text{NOMA}} \\ R_{\text{sum}}^{\text{Hybrid}} & P_{\text{out}}^{\text{Hybrid}} & \mathcal{F}^{\text{Hybrid}} \end{bmatrix}.$$

- Step 3: construct the normalized evaluation matrix, $\mathbf{N} = (n_{ij})_{3\times 3}$, using the following formula:

$$n_{ij} = \frac{\delta_{ij}}{\sqrt{\sum_{k=1}^{3}\delta_{kj}^2}}, \quad \forall i = 1, 2, 3.$$

- Step 4: assign a weight to each attribute based on its relative importance. The importance of a specific attribute can be decided based on the overall system requirements. For example, if the aim is to maximize the achievable sum rate, the sum rate attribute is given a higher weight and vice versa. It is also possible to give equal weights for different attributes, or a zero weight in case an attribute is not considered. Let the weight for attribute j be ϖ_j, the weighted decision matrix can be constructed as $\mathbf{W} = (w_{ij})_{3\times 3}$, where $w_{ij} = \varpi_j n_{ij}$.
- Step 5: determine the best alternative, $A_{\text{b}} = (a_{\text{b}})_{3\times 1}$ and the worst alternative, $A_{\text{w}} = (a_{\text{w}})_{3\times 1}$ with respect to each criterion on the weighted normalized decision matrix, as follows:

$$a_{\text{b}j} = \begin{cases} \min(w_{ij}|i = 1, 2, 3) & j \in J_- \\ \max(w_{ij}|i = 1, 2, 3) & j \in J_+, \end{cases}$$

$$a_{\text{w}j} = \begin{cases} \max(w_{ij}|i = 1, 2, 3) & j \in J_- \\ \min(w_{ij}|i = 1, 2, 3) & j \in J_+, \end{cases}$$

where J_+ is associated with benefit criteria, i.e., sum rate and fairness index, whereas J_- is associated with cost criteria, i.e., outage probability.
- Step 6: determine the separation from PIS, $S_{\text{p}} = (s_{\text{p}_i})_{3\times 1}$, and the separation from NIS, $S_{\text{n}} = (s_{\text{n}i})_{3\times 1}$, based on L2-distance between the target alternative and

TABLE 1. Complexity evaluation.

Step	Step Complexity
construction of the evaluation matrix	$O(n) \times O(m)$
attribute normalization and weighing	$O(n) \times O(m) + O(m)$
determine PIS and NIS	$O(m) + O(m)$
calculate seperation from PIS and NIS	$O(m) \times O(n) + O(m) \times O(n)$
rank the alternatives	$O(1)$
Total Complexity	$O(nm) + O(nm) + O(nm) + O(m) + O(m) + O(1) = O(nm)$

the best and worst alternatives, respectively, such that:

$$s_{\text{p}i} = \sqrt{\sum_{j=1}^{3}(w_{ij} - a_{bj})^2},$$

and

$$s_{\text{n}i} = \sqrt{\sum_{j=1}^{3}(w_{ij} - a_{wj})^2}.$$

• Step 7: rank the alternatives according to the distances from the best and the worst solutions. To do so, the distance from NIS is divided by the summation of PIS and NIS. As a result, the ranked alternatives vector can be constructed as:

$$R = \text{rank}\left[\frac{S_{\text{n}}}{S_{\text{p}} + S_{\text{n}}}\right],$$

the first ranked alternative is then chosen as a MA scheme.

D. COMPLEXITY EVALUATION
We evaluate the complexity of the proposed DMAS scheme using Big O notation. Table 1 shows the complexity of each step involved in the DMAS decision making process as well as the total complexity, where n and m denote the number of multiple access alternatives and attributes, respectively. Given that the proposed DMAS scheme works on 3 possible alternatives, namely: OMA, NOMA and hybrid, the resulting complexity can be expressed as $O(3m)$. Hence, the higher the number of evaluation attributes required in the system design, the higher the computational complexity of DMAS.

V. ATTRIBUTES EVALUATION
In this section, we present the performance metrics used to form the attributes evaluation matrix in (19). Specifically, we derive the sum rate, outage probability and Jain's fairness index for each of the three MA modes under consideration,

assuming the attocell users are uniformly distributed over the coverage area [27], [32].

A. SUM RATE
In the adopted framework, the AP evaluates the expected achievable sum rate for each alternative MA scheme based on the knowledge of users' polar coordinates. It was shown in [41] that trough symbol shaping and coding, the OFDM-based optical signals can achieve Shannon capacity. To this end, the data rate for the k-th user is:

$$R_k = \sum_{n=1}^{N_k} b(n) \log_2(1 + \gamma_k(n)), \tag{19}$$

where $b(n)$ is the bandwidth of subcarrier n. Also, N_k donates the average number of information-bearing subcarriers per user, which can be calculated as follows for the different MA schemes:

$$N_k = \begin{cases} \dfrac{(N_{\text{FFT}} - 2)}{2\,KN_{\text{FFT}}} & \text{for OMA} \\[2mm] \dfrac{(N_{\text{FFT}} - 2)}{2\,N_{\text{FFT}}} & \text{for NOMA} \\[2mm] \dfrac{(N_{\text{FFT}} - 2)}{2(N_{\text{pairs}} + N_{\text{unpaired}})N_{\text{FFT}}} & \text{for Hybrid} \end{cases} \tag{20}$$

consequently, the total achievable sum rate can be calculated as $R_{\text{sum}} = \sum_{k=1}^{K} \mathbb{E}[R_k]$. The sum rate expressions for the three different MA schemes are listed in Table 2 below.

B. OUTAGE PROBABILITY
To guarantee the QoS required by the attocell users, we define ϵ_A and ϵ_B as the minimum received SINR required by the cell-centre and cell-edge users, respectively. For the sake of simplicity, front-end devices filtering effect is not included in the outage expressions. The user's outage probability based on its location can be expressed as:

$$P_{\text{out}_k} = \begin{cases} \Pr[\gamma_k < \epsilon_A] & r_k \leq r_A \\ \Pr[\gamma_k < \epsilon_B] & r_A < r_k \leq r_B \end{cases}$$

TABLE 2. Sum rate expressions for the different MA alternatives.

Notation	Calculation
$R_{\text{sum}}^{\text{OMA}}$	$\sum_{k=1}^{K} \sum_{n=1}^{N_k} b(n) \log_2 \left(1 + \dfrac{\exp(-\frac{nF_s}{N_{\text{FFT}}F_{\text{fe}}})\zeta^2 \eta_{\text{PD}}^2 P_{\text{elec}}^2}{\sigma_{\text{Rx}}^2 (r_k^2 + z^2)^{m+3}} \right)$
$R_{\text{sum}}^{\text{NOMA}}$	$\sum_{n=1}^{N_K} b(n) \log_2 \left(1 + \dfrac{\exp(-\frac{nF_s}{N_{\text{FFT}}F_{\text{fe}}})\zeta^2 \eta_{\text{PD}}^2 P_{\text{elec}}^2 P_K^2}{\sigma_{\text{Rx}}^2 (r_k^2 + z^2)^{m+3}} \right) +$ $\sum_{k=1}^{K-1} \sum_{n=1}^{N_k} b(n) \log_2 \left(1 + \left(\dfrac{\sum_{i=k}^{K} P_i^2}{P_k^2} + \dfrac{\sigma_{\text{Rx}}^2 (r_k^2 + z^2)^{m+3}}{\exp(-\frac{nF_s}{N_{\text{FFT}}F_{\text{fe}}})\zeta^2 \eta_{\text{PD}}^2 P_{\text{elec}}^2 P_k^2} \right)^{-1} \right)$
$R_{\text{sum}}^{\text{Hybrid}}$	$\sum_{k=1}^{N_{\text{unpaired}}} \sum_{n=1}^{N_k} b(n) \log_2 \left(1 + \dfrac{\exp(-\frac{nF_s}{N_{\text{FFT}}F_{\text{fe}}})\zeta^2 \eta_{\text{PD}}^2 P_{\text{LED}}^2}{\sigma_{\text{Rx}}^2 (r_k^2 + z^2)^{m+3}} \right) +$ $\sum_{i=1}^{N_{\text{pairs}}} \left(\sum_{n=1}^{N_{i_2}} b(n) \log_2 \left(1 + \dfrac{\exp(-\frac{nF_s}{N_{\text{FFT}}F_{\text{fe}}})\eta_{\text{PD}}^2 P_{\text{LED}}^2 \zeta^2 \eta_{\text{PD}}^2 P_{\text{LED}}^2 P_{i_2}^2}{(r_{i_2}^2 + z^2)^{m+3} \sigma_{\text{Rx}}^2} \right) + \right.$ $\left. \sum_{n=1}^{N_{i_1}} b(n) \log_2 \left(1 + \left(\dfrac{P_{i_2}^2}{P_{i_1}^2} + \dfrac{\sigma_{\text{Rx}}^2 (r_k^2 + z^2)^{m+3}}{\exp(-\frac{nF_s}{N_{\text{FFT}}F_{\text{fe}}})\zeta^2 \eta_{\text{PD}}^2 P_{\text{elec}}^2 P_{i_1}^2} \right)^{-1} \right) \right)$

where $\gamma_k = \frac{1}{N_k} \sum_{n=1}^{N_k} \gamma_k(n)$, and the SINR per subcarrier, $\gamma_k(n)$ is obtained from (14), (16), (17) and (18) for the different MA modes. Thus, the outage probability can be easily calculated using the SINR expressions derived earlier. For example, under OMA, the user outage probability for cell-centre user k_A, where $r_k \leq r_A$, can be obtained as:

$$P_{\text{out}_{k_A}}^{\text{OMA}} = \Pr \left[\frac{\zeta^2 \eta_{\text{PD}}^2 P_{\text{elec}}^2}{\sigma_{\text{Rx}}^2 (r_k^2 + z^2)^{m+3}} < \epsilon_A \right]$$

$$= 1 - \Pr \left[r_k < \sqrt{\left(\frac{\zeta^2 \eta_{\text{PD}}^2 P_{\text{elec}}^2}{\sigma_{\text{Rx}}^2 \epsilon_A} \right)^{\frac{1}{m+3}} - z^2} \right]$$

$$= 1 - \int_0^{\left(\left(\frac{\zeta^2 \eta_{\text{PD}}^2 P_{\text{elec}}^2}{\sigma_{\text{Rx}}^2 \epsilon_A} \right)^{\frac{1}{m+3}} - z^2 \right)^{\frac{1}{2}}} f_R(r) dr, \quad (21)$$

where $f_R(r) = 2r/r_B^2$ is the PDF of variable r_k following the uniform distribution. Hence the outage probability for cell-centre users can be calculated as:

$$P_{\text{out}_{k_A}}^{\text{OMA}} = 1 + \frac{z^2}{r_B^2} - \frac{1}{r_B^2} \left(\frac{\zeta^2 \eta_{\text{PD}}^2 P_{\text{elec}}^2}{\sigma_{\text{Rx}}^2 \epsilon_A} \right)^{\frac{1}{m+3}},$$

similarly, the outage probability for cell-edge user, k_B, can be calculated as:

$$P_{\text{out}_{k_B}}^{\text{OMA}} = \Pr \left[\frac{\zeta^2 \eta_{\text{PD}}^2 P_{\text{elec}}^2}{\sigma_{\text{Rx}}^2 (r_k^2 + z^2)^{m+3}} < \epsilon_B \right]$$

$$= 1 - \Pr \left[r_k < \sqrt{\left(\frac{\zeta^2 \eta_{\text{PD}}^2 P_{\text{elec}}^2}{\sigma_{\text{Rx}}^2 \epsilon_B} \right)^{\frac{1}{m+3}} - z^2} \right]$$

$$= 1 - \int_{r_A}^{\left(\left(\frac{\zeta^2 \eta_{\text{PD}}^2 P_{\text{elec}}^2}{\sigma_{\text{Rx}}^2 \epsilon_A} \right)^{\frac{1}{m+3}} - z^2 \right)^{\frac{1}{2}}} f_R(r) dr$$

$$= 1 + \frac{z^2}{r_B^2} + \frac{r_A^2}{r_B^2} - \frac{1}{r_B^2} \left(\frac{\zeta^2 \eta_{\text{PD}}^2 P_{\text{elec}}^2}{\sigma_{\text{Rx}}^2 \epsilon_A} \right)^{\frac{1}{m+3}}, \quad (22)$$

as a result, the overall outage probability for OMA users can be calculated as:

$$P_{\text{out}}^{\text{OMA}}$$
$$= \Pr[r_k \leq r_A] \times P_{\text{out}_{k_A}}^{\text{OMA}} + \Pr[r_A < r_k \leq r_B] \times P_{\text{out}_{k_B}}^{\text{OMA}}$$

$$= \frac{r_A^2}{r_B^2} \left(1 + \frac{z^2}{r_B^2} - \frac{1}{r_B^2} \left(\frac{\zeta^2 \eta_{\text{PD}}^2 P_{\text{elec}}^2}{\sigma_{\text{Rx}}^2 \epsilon_A} \right)^{\frac{1}{m+3}} \right)$$

$$+ \left(1 - \frac{r_A^2}{r_B^2} \right) \left(1 + \frac{z^2}{r_B^2} + \frac{r_A^2}{r_B^2} - \frac{1}{r_B^2} \left(\frac{\zeta^2 \eta_{\text{PD}}^2 P_{\text{elec}}^2}{\sigma_{\text{Rx}}^2 \epsilon_A} \right)^{\frac{1}{m+3}} \right). \quad (23)$$

Following the same principle, the outage probabilities under the three different MA schemes can be obtained as in Table 3 below. It is noted that when NOMA mode is applied, the user with highest decoding order, U_K, has the most favourable channel gain, i.e., $r_K \leq r_k$ for $k = 1, 2, \ldots, K - 1$, and thus it is assigned the lowest power allocation coefficient. As a result, service satisfaction at U_K requires that it successfully decodes and subtracts the signals of other users. Assuming perfect SIC is performed, U_K can decode its signal without residual interference. Other attocell users, however, need to decode their signals with the existence of interference from users with a higher decoding order. The average user outage

TABLE 3. Average user outage probability for the different MA alternatives.

Notation	Calculation
$\mathrm{P_{out}^{OMA}}$	$\frac{r_A^2}{r_B^2}\left[1+\frac{z^2}{r_B^2}-\frac{1}{r_B^2}\left(\frac{\varsigma^2\eta_{\mathrm{PD}}^2 P_{\mathrm{elec}}^2}{\sigma_{\mathrm{Rx}}^2\epsilon_A}\right)^{\frac{1}{m+3}}\right]+\left(1-\frac{r_A^2}{r_B^2}\right)\left[1+\frac{z^2}{r_B^2}+\frac{r_A^2}{r_B^2}-\frac{1}{r_B^2}\left(\frac{\varsigma^2\eta_{\mathrm{PD}}^2 P_{\mathrm{elec}}^2}{\sigma_{\mathrm{Rx}}^2\epsilon_A}\right)^{\frac{1}{m+3}}\right]$
$P_{\mathrm{out}}^{\mathrm{NOMA}}$	$\frac{1}{K}\left[1+\frac{z^2}{r_B^2}-\frac{1}{r_B^2}\left(\frac{\varsigma^2\eta_{\mathrm{PD}}^2 P_{\mathrm{elec}}^2 P_K^2}{\sigma_{\mathrm{Rx}}^2\epsilon_A}\right)^{\frac{1}{m+3}}\right]+\left(\frac{r_A^2}{r_B^2}-\frac{1}{K}\right)\left[1+\frac{z^2}{r_B^2}-\frac{1}{r_B^2}\left(\frac{\varsigma^2\eta_{\mathrm{PD}}^2 P_{\mathrm{elec}}^2 P_k^2}{\epsilon_A\sigma_{\mathrm{Rx}}^2}-\frac{\varsigma^2\eta_{\mathrm{PD}}^2 P_{\mathrm{elec}}^2\sum_{i=k+1}^K P_i^2}{\sigma_{\mathrm{Rx}}^2}\right)^{\frac{1}{m+3}}\right]$ $+\left(1-\frac{r_A^2}{r_B^2}\right)\left[1+\frac{z^2}{r_B^2}+\frac{r_A^2}{r_B^2}-\frac{1}{r_B^2}\left(\frac{\varsigma^2\eta_{\mathrm{PD}}^2 P_{\mathrm{elec}}^2 P_k^2}{\epsilon_B\sigma_{\mathrm{Rx}}^2}-\frac{\varsigma^2\eta_{\mathrm{PD}}^2 P_{\mathrm{elec}}^2\sum_{i=k+1}^K P_i^2}{\sigma_{\mathrm{Rx}}^2}\right)^{\frac{1}{m+3}}\right]$
$\mathrm{P_{out}^{Hybrid}}$	$\frac{N_{\mathrm{pairs}}}{2K}\left[\left(1+\frac{z^2}{r_B^2}-\frac{1}{r_B^2}\left(\frac{\varsigma^2\eta_{\mathrm{PD}}^2 P_{\mathrm{elec}}^2 P_2^2}{\sigma_{\mathrm{Rx}}^2\epsilon_A}\right)^{\frac{1}{m+3}}\right)+\left(1+\frac{z^2}{r_B^2}+\frac{r_A^2}{r_B^2}-\frac{1}{r_B^2}\left(\frac{\varsigma^2\eta_{\mathrm{PD}}^2 P_{\mathrm{elec}}^2 P_1^2}{\epsilon_B\sigma_{\mathrm{Rx}}^2}-\frac{\varsigma^2\eta_{\mathrm{PD}}^2 P_{\mathrm{elec}}^2 P_2^2}{\sigma_{\mathrm{Rx}}^2}\right)^{\frac{1}{m+3}}\right)\right]$ $\frac{N_{\mathrm{unpaired}}}{K}\left[\frac{r_A^2}{r_B^2}\left(1+\frac{z^2}{r_A^2}-\frac{1}{r_A^2}\left(\frac{\varsigma^2\eta_{\mathrm{PD}}^2 P_{\mathrm{elec}}^2}{\sigma_{\mathrm{Rx}}^2\epsilon_A}\right)^{\frac{1}{m+3}}\right)+\left(1-\frac{r_A^2}{r_B^2}\right)\left(1+\frac{z^2}{r_B^2}+\frac{r_A^2}{r_B^2}-\frac{1}{r_B^2}\left(\frac{\varsigma^2\eta_{\mathrm{PD}}^2 P_{\mathrm{elec}}^2}{\sigma_{\mathrm{Rx}}^2\epsilon_A}\right)^{\frac{1}{m+3}}\right)\right]$

TABLE 4. Jain's fairness index for the different MA alternatives.

Notation	Calculation
$\mathcal{F}^{\mathrm{OMA}}$	$R_{\mathrm{OMA}}^{\mathrm{sum}^2}\Big/\left[K\sum_{k=1}^K\left(\sum_{n=1}^{N_k}b(n)\log_2\left(1+\frac{\exp(-\frac{nF_s}{N_{\mathrm{FFT}}F_{\mathrm{fe}}})\varsigma^2\eta_{\mathrm{PD}}^2 P_{\mathrm{elec}}^2}{\sigma_{\mathrm{Rx}}^2(r_k^2+z^2)^{m+3}}\right)\right)^2\right]$
$\mathcal{F}^{\mathrm{NOMA}}$	$R_{\mathrm{NOMA}}^{\mathrm{sum}^2}\Big/\left[\left(\sum_{n=1}^{N_K}b(n)\log_2\left(1+\frac{\exp(-\frac{nF_s}{N_{\mathrm{FFT}}F_{\mathrm{fe}}})\varsigma^2\eta_{\mathrm{PD}}^2 P_{\mathrm{elec}}^2 P_K^2}{\sigma_{\mathrm{Rx}}^2(r_k^2+z^2)^{m+3}}\right)\right)^2+\right.$ $\left.\sum_{k=1}^{K-1}\left(\sum_{n=1}^{N_k}b(n)\log_2\left(1+\left(\frac{\sum_{i=k}^K P_i^2}{P_k^2}+\frac{\sigma_{\mathrm{Rx}}^2(r_k^2+z^2)^{m+3}}{\exp(-\frac{nF_s}{N_{\mathrm{FFT}}F_{\mathrm{fe}}})\varsigma^2\eta_{\mathrm{PD}}^2 P_{\mathrm{elec}}^2 P_k^2}\right)^{-1}\right)\right)^2\right]$
$\mathcal{F}^{\mathrm{Hybrid}}$	$R_{\mathrm{Hybrid}}^{\mathrm{sum}^2}\Big/\left[\sum_{k=1}^{N_{\mathrm{unpaired}}}\left(\sum_{n=1}^{N_k}b(n)\log_2\left(1+\frac{\exp(-\frac{nF_s}{N_{\mathrm{FFT}}F_{\mathrm{fe}}})\varsigma^2\eta_{\mathrm{PD}}^2 P_{\mathrm{LED}}^2}{\sigma_{\mathrm{Rx}}^2(r_k^2+z^2)^{m+3}}\right)\right)^2+\right.$ $\sum_{i=1}^{N_{\mathrm{pairs}}}\left(\sum_{n=1}^{N_{i_2}}b(n)\log_2\left(1+\frac{\exp(-\frac{nF_s}{N_{\mathrm{FFT}}F_{\mathrm{fe}}})\eta_{\mathrm{PD}}^2 P_{\mathrm{LED}}^2\varsigma^2\eta_{\mathrm{PD}}^2 P_{\mathrm{LED}}^2 P_{i_2}^2}{(r_{i_2}^2+z^2)^{m+3}\sigma_{\mathrm{Rx}}^2}\right)\right)^2+$ $\left.\sum_{i=1}^{N_{\mathrm{pairs}}}\left(\sum_{n=1}^{N_i}b(n)\log_2\left(1+\left(\frac{P_{i_1}^2}{P_{i_2}^2}+\frac{\sigma_{\mathrm{Rx}}^2(r_k^2+z^2)^{m+3}}{\exp(-\frac{nF_s}{N_{\mathrm{FFT}}F_{\mathrm{fe}}})\varsigma^2\eta_{\mathrm{PD}}^2 P_{\mathrm{elec}}^2 P_k^2}\right)^{-1}\right)\right)^2\right]$

probability under NOMA can then be calculated as:

$$\mathrm{P_{out}^{NOMA}}=\frac{1}{K}\mathrm{P_{out_K}^{NOMA}}+\left(\frac{r_A^2}{r_B^2}-\frac{1}{K}\right)\mathrm{P_{out_{k_A}}^{NOMA}}+\left(1-\frac{r_A^2}{r_B^2}\right)\mathrm{P_{out_{k_B}}^{NOMA}},$$

where $\mathrm{P_{out_K}^{NOMA}}$ donates the outage probability of the user with highest decoding order, and $\mathrm{P_{out_{k_A}}^{NOMA}}$ and $\mathrm{P_{out_{k_B}}^{NOMA}}$ are the outage probabilities of the cell-centre and cell-edge users, respectively, with the presence of interference. Moreover, under the hybrid mode, each cell edge user is paired with a cell centre user and their signals are multiplexed in the power domain. Unpaired users, if any, are then allocated separate subcarriers. As a result, the average user outage probability can be calculated as:

$$\mathrm{P_{out}^{Hybrid}}=\frac{N_{\mathrm{pairs}}}{K}\mathrm{P_{out}^{pairs}}+\frac{N_{\mathrm{unpaired}}}{K}\mathrm{P_{out}^{unpaired}},$$

where $\mathrm{P_{out}^{pairs}}$ and $\mathrm{P_{out}^{unpaired}}$ denote the outage probability for paired and unpaired users, respectively, which yields the expression shown in Table 3.

C. USER FAIRNESS

We consider throughput fairness among the attocell users for quantifying the notion of resource allocation fairness. To this end, we adopt Jain's index fairness measure which characterizes the contribution of the individual data rate of users to the system sum rate [42]. Throughput Jain-fairness index can be evaluated as:
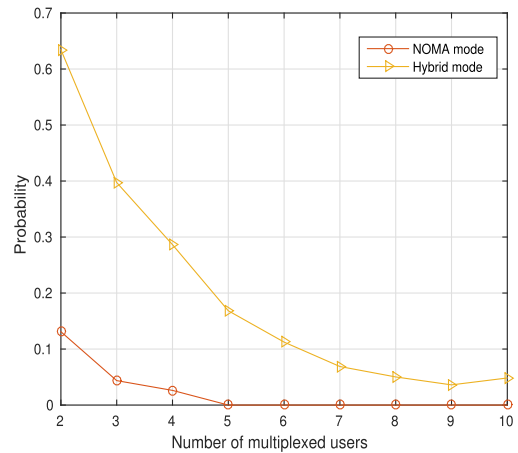
$$\mathcal{F}=\frac{\left(\sum_{k=1}^K R_k\right)^2}{K\sum_{k=1}^K R_k^2}, \tag{24}$$

(a) (b) (c)
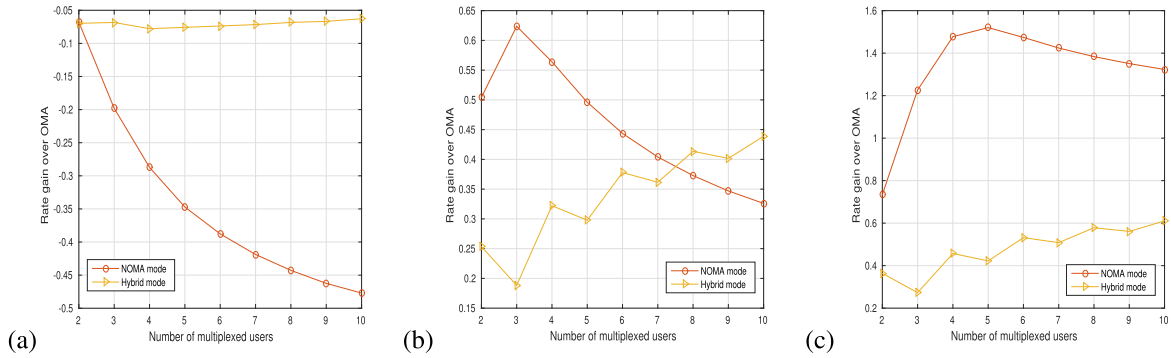
FIGURE 4. Comparison of average achievable rate gain over OMA between NOMA and hybrid modes under a transmit SNR of (a) 100 dB, (b) 120 dB, and (c) 140 dB.

TABLE 5. Simulation parameters.

Description	Notation	Value
PD responsivity	η_{PD}	0.4 A/W
Transmitter semi-angle	φ_k	60 deg
FOV of the PDs	ϕ_{c_k}	60 deg
Attocell radius	r_B	4.0 m
Attocell-centre radius	r_A	2.0 m
Vertical distance	z	2.15 m
Physical area of PD	A_k	1.0 cm^2
Refractive index of PD lens	n	1.5
Gain of optical filter	$T_s(\phi_k)$	1.0
Bandwidth	B	20 Mbps
Maximum number of users	K	10
Total Number of subcarriers	N_{FFT}	128
QAM modulation order	M	4
Power allocation factor	α	0.3

which can be easily calculated based on the rate analysis presented earlier as shown in Table 4 below, where $R_{\text{OMA}}^{\text{sum}}$, $R_{\text{NOMA}}^{\text{sum}}$ and $R_{\text{Hybrid}}^{\text{sum}}$ denote the achievable sum rate under OMA, NOMA and hybrid modes, respectively. According to (24), the value of $\mathcal{F}$ is bounded by $[\frac{1}{K}, 1]$, where a greater Jain's index corresponds to a fairer system and maximum fairness is achieved when all the users obtain the same individual data rate.

VI. SIMULATION RESULTS

In this section, we present the simulation results for the system and channel models presented in Section II. Without loss of generality, we consider an attocell AP located in the centre of a room, with a cell radius, $r_B = 4$ m. To this end, the cell-centre boundary is assumed to be a circle with radius $r_A = 2$ m, while the cell-edge is formed by the ring bounded by r_A and r_B. Also, we assume that a maximum


FIGURE 5. The probability of NOMA and hybrid modes being fairer than OMA versus the number of multiplexed users.

of 10 uniformly distributed users may exist in the coverage area of the attocell AP, and that MA can be provided by one of the three modes discussed is Section III, namely: OMA, NOMA and hybrid OMA/NOMA. Unless otherwise specified, the system parameters used for the simulations are listed in Table 5. First, we investigate the performance of the different MA modes presented in the paper. Fig. 4 shows the rate gain of NOMA and hybrid modes over OMA, which are defined as $\eta^{\text{NOMA}} = (R_{\text{sum}}^{\text{NOMA}} - R_{\text{sum}}^{\text{OMA}})/R_{\text{sum}}^{\text{OMA}}$ and $\eta^{\text{Hybrid}} = (R_{\text{sum}}^{\text{Hybrid}} - R_{\text{sum}}^{\text{OMA}})/R_{\text{sum}}^{\text{OMA}}$, respectively. It can be seen that both NOMA and hybrid modes fail to achieve any rate gain over OMA in the case of low transmit SNR of 100 dB as seen in Fig. 4 (a). In fact, multiplexing all users in the power domain leads to severe sum rate degradation to almost half of the OMA rate when the number of multiplexed users is 10. For a higher transmit SNR of 120 dB, NOMA achieves maximum rate gain for 3 multiplexed users and then exhibits rate degradation as the number of users increases. This is due to interference cancellation errors at users with a high decoding order as well as the high interference affecting users with a low decoding order. It is noted that hybrid mode outperforms NOMA for a number of 8 or more multiplexed users. It is also
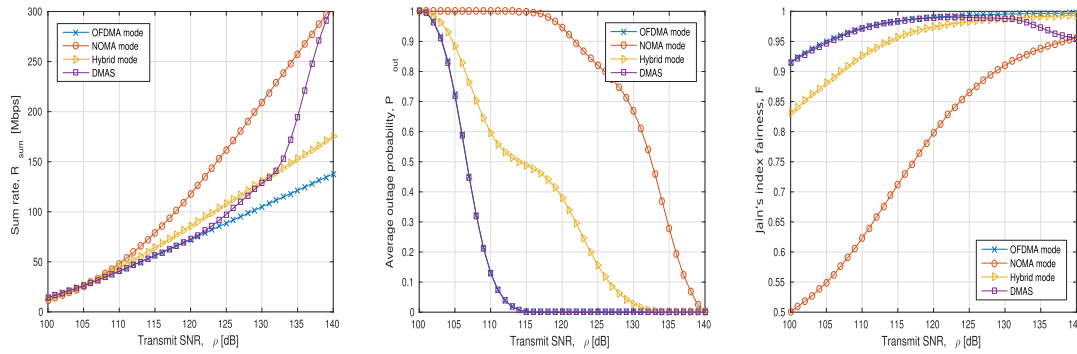
FIGURE 6. Achieved performance under the different MA schemes compared to the proposed DMAS with $[\varpi_{R_{sum}}, \varpi_{P_{out}}, \varpi_{\mathcal{F}}] = [0.4, 0.3, 0.3]$ for a system with 3 multiplexed users.
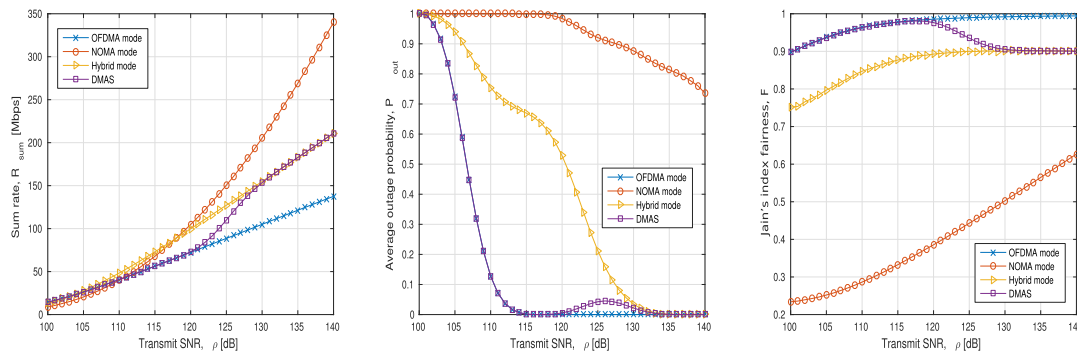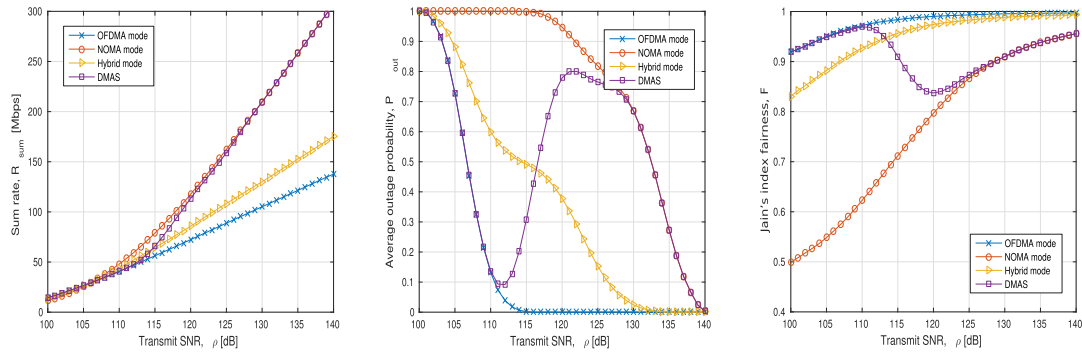

FIGURE 7. Achieved performance under the different MA schemes compared to the proposed DMAS with $[\varpi_{R_{sum}}, \varpi_{P_{out}}, \varpi_{\mathcal{F}}] = [0.4, 0.3, 0.3]$ for a system with 6 multiplexed users.

noted that the ripple effect in the rate gain of the hybrid mode is because the hybrid mode provides more rate gain for even numbers of multiplexed users; as there is a higher probability of pairing all users in this case. As seen in Fig. 4 (b), the rate of the hybrid mode is not equivalent to the rate of NOMA with 2 users. This is because the hybrid mode pairs the two users only when they exhibit distinctive channel conditions, while NOMA always performs power-domain multiplexing regardless of the channel conditions of the users. The rate gain of NOMA over OMA is most evident when a high transmit SNR of 140 dB is assumed as shown is Fig 4 (c). This outcome is consistent with the conclusion drawn in [45], which states that the performance gain of NOMA is more resistant to the impact of imperfect SIC in high SNR regime, while the gain of NOMA completely vanishes when 6% or more inter-user NOMA interference fails to be eliminated, i.e., due to low SINR.

Next, we investigate the fairness provided by the different MA schemes. Given that equal AAP is assumed, it is expected that OMA provides the best user fairness for high numbers of users. This is because power domain multiplexing necessitates that users with a low decoding order decode their signals with the presence of interference, leading to low SINR values at these users. Thus, it is acceptable in NOMA that users with less favourable channel conditions

suffer high interference while users close to the AP can eliminate multi-user interference by means of SIC. Fig. 5 shows the probability that NOMA and hybrid modes achieve better fairness than OMA (in terms of Jain's index) versus the number of multiplexed users. These values are obtained by averaging the probabilities over a transmit SNR range of 100 dB to 140 dB. It is evident that NOMA can achieve better fairness than OMA with very low probability, i.e., about 0.1 probability only when a small number of multiplexed users is assumed. In addition, we can observe that hybrid mode has a higher probability of being fairer than OMA for small numbers of users. It is worth noting here that the probability of NOMA being fairer than OMA is much lower than that of the hybrid mode for the case of two multiplexed users. This is due to the pairing strategy in hybrid mode which allows power domain multiplexing only when the two users have distinctive channel conditions, i.e., one lies in the cell centre while the other is located near the cell edge.

Next, we investigate the system performance under the three MA modes as well as the proposed DMAS. For these results, we assume that the minimum required SINR values at cell-centre and cell-edge users are $\epsilon_A = 10$ dB and $\epsilon_A = 8$ dB, respectively. Fig. 6 and Fig. 7 show the achievable sum rate, average outage probability and Jain's index for a system with 3 and 6 multiplexed users, respectively. For

FIGURE 8. Achieved performance under the different MA schemes compared to the proposed DMAS with $[\varpi_{R_{sum}}, \varpi_{P_{out}}, \varpi_{\mathcal{F}}] = [0.8, 0.2, 0]$ for a system with 3 multiplexed users.
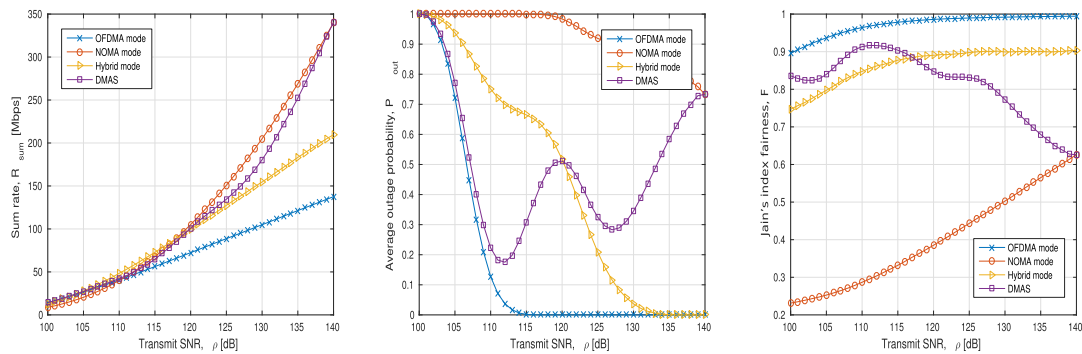

FIGURE 9. Achieved performance under the different MA schemes compared to the proposed DMAS with $[\varpi_{R_{sum}}, \varpi_{P_{out}}, \varpi_{\mathcal{F}}] = [0.8, 0.2, 0]$ for a system with 6 multiplexed users.

these results, the attributes' weights for DMAS are set to $[\varpi_{R_{sum}}, \varpi_{P_{out}}, \varpi_{\mathcal{F}}] = [0.4, 0.3, 0.3]$. Thus, the three performance metrics are given similar weights. As seen in Fig. 6, NOMA can achieve the highest sum rate due to performing power domain multiplexing over all available subcarriers. This, however, comes with inevitable cost of increased average user outage probability which is particularly clear for the case of 6 multiplexed users in Fig. 7. This is due to the high interference affecting users with low decoding orders. Also, it is clear that NOMA mode provides the lowest fairness among users. This can be interpreted by the fact that NOMA allocates different power values to the different users, leading to big differences in the achievable individual data rates. It can be seen also that OMA mode provides the lowest achievable sum rate with the best outage probability and fairness performance, while hybrid mode finds a trade-off between OMA and NOMA. The hybrid mode, however, does not count for specific system requirements and cannot be dynamically adapted. To this end, the proposed DMAS chooses among the three modes based on the given attributes' weights. It is seen, for example, that for the case of 3 users, DMAS chooses OMA for the low SNR region, hybrid for medium SNR values while it applies NOMA for high SNRs only. For the scenario with 6 multiplexed users, DMAS chooses OMA and hybrid modes depending on the SNR values, while the NOMA mode

is not applied. This is due to the almost equal weights given to the three performance attributes, including outage probability which can be highly degraded under NOMA for high numbers of users.

Next, we show in Fig. 8 and Fig. 9 the achievable system performance for 3 and 6 multiplexed users when the attributes' weights are set to $[\varpi_{R_{sum}}, \varpi_{P_{out}}, \varpi_{\mathcal{F}}] = [0.8, 0.2, 0]$. Here, the fairness metric is ignored and higher weight is given to the sum rate. It can be inferred from the presented results that the proposed DMAS prioritizes sum rate and thus tends to apply NOMA in the high SNR region even in the scenario with 6 multiplexed users in Fig. 9.

In order to demonstrate the probability of choosing each of the MA alternatives under various conditions, Fig. 10 shows the probability that DMAS applies each of the three candidate modes for different SNR values and different numbers of users. In Fig. 10 (a), the attributes' weights are set to $[\varpi_{R_{sum}}, \varpi_{P_{out}}, \varpi_{\mathcal{F}}] = [0.4, 0.3, 0.3]$ while Fig. 10 (b) shows the results when the weights are set to $[\varpi_{R_{sum}}, \varpi_{P_{out}}, \varpi_{\mathcal{F}}] = [0.8, 0.2, 0]$. For the first set of weights, all of the three attributes are given similar importance, and hence, the proposed DMAS finds a balance between throughput, outage and fairness. As a result, OMA mode is applied with high probability when the number of multiplexed users is high
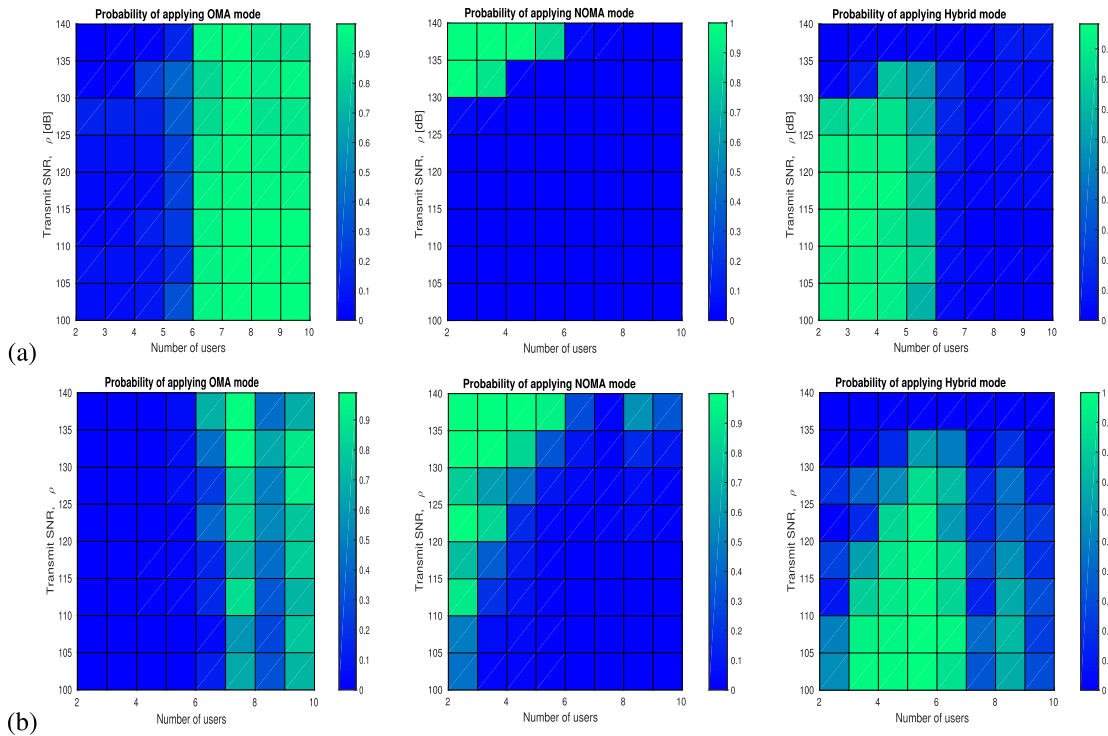
FIGURE 10. Probability that DMAS with (a) $[\varpi_{R_\text{sum}}, \varpi_{P_\text{out}}, \varpi_\mathcal{F}] = [0.4, 0.3, 0.3]$ and (b) $[\varpi_{R_\text{sum}}, \varpi_{P_\text{out}}, \varpi_\mathcal{F}] = [0.8, 0.2, 0]$ applies OMA mode, NOMA mode and hybrid mode for different numbers of users and transmit SNR values.
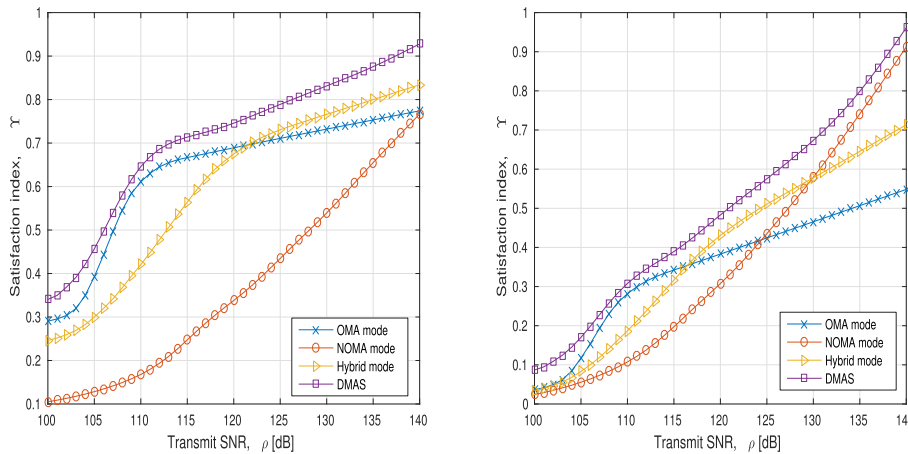
FIGURE 11. Satisfaction index of the proposed DMAS with (a) $[\varpi_{R_\text{sum}}, \varpi_{P_\text{out}}, \varpi_\mathcal{F}] = [0.4, 0.3, 0.3]$ and (b) $[\varpi_{R_\text{sum}}, \varpi_{P_\text{out}}, \varpi_\mathcal{F}] = [0.8, 0.2, 0]$ compared to the different MA modes.

(6 users or more). This can be interpreted by the results shown in Fig. 5 which indicate that NOMA and hybrid modes can achieve better fairness than OMA only for small numbers of multiplexed users. It can also be seen from Fig. 10 (a) that DMAS chooses NOMA only in the high SNR region to ensure that the QoS requirements for all users are satisfied. On the contrast, we can see from Fig. 10 (b) that DMAS applies NOMA with high probability for small numbers of users even in the low SNR region. This is because the attributes weights in this scenario do not require fairness to be ensured among

users. From the presented results we can conclude that the proposed DMAS provides a simple and cost-effective solution to determine the best MA alternative for given system requirements. In order to evaluate the degree to which the proposed DMAS satisfies system requirements, we define the system satisfaction index as follows:

$$\Upsilon = \varpi_{R_\text{sum}} \times \frac{R_\text{sum}}{\Lambda} + \varpi_{P_\text{out}} \times \left(1 - \frac{P_\text{out}}{\Xi}\right) + \varpi_\mathcal{F} \times \frac{\mathcal{F}}{\Pi},$$

(25)

where Λ, Ξ and Π donate the required system sum rate, outage probability and Jain's fairness index, respectively. Fig. 11 shows the satisfaction index, Υ, for the proposed DMAS scheme compared to static MA modes. These results are obtained from averaging 10^5 channel realizations for random numbers of uniformly distributed users inside the AP coverage area. It can be inferred from the figure that the value of Υ increases for higher SNRs, i.e., the AP can better accommodate the QoS requirements in this case. It is also clear that the proposed DMAS provides the highest possible satisfaction index over the entire SNR range. Thus, DMAS outperforms static MA configuration in accommodating the QoS requirements of the LiFi AP users.

VII. CONCLUSION

This paper proposed DMAS as an autonomous MA selection scheme that aims to minimize user intervention and enable self-configuration in intelligent LiFi attocell APs. To this end, DMAS imparts the subjective evaluation of various MA schemes, namely OMA, NOMA and hybrid OMA/NOMA, based on the computational evaluation of the sum rate, outage and fairness criteria. Furthermore, DMAS can be dynamically configured to support diverse LiFi use cases by carefully assigning weights to the attributes in the developed multi-criteria decision techniques. The presented simulation results showed that DMAS provides effective decision-making on the best MA alternative under various users' densities and demands. For instance, DMAS has been shown to decide on adopting an OMA scheme when a high number of users (e.g., more than 6 users) attempted to simultaneously access the network. Whereas a NOMA scheme was adopted for small numbers of users only when the SNR range allowed for reliable detection at the receiving terminals. It was also demonstrated that the proposed DMAS provides the highest system satisfaction index compared to the static configuration of a single MA scheme. This is maintained regardless of the given attributes' weights or SNR values. We believe that the proposed framework can enable the design goal of "anything as a service" in future 5G networks, and can be possibly extended to include combinations of various design attributes and configurable alternatives to shape many LiFi applications in different sectors.

REFERENCES

[1] H. Haas, L. Yin, Y. Wang, and C. Chen, "What is LiFi?" *J. Lightw. Technol.*, vol. 34, no. 6, pp. 1533–1544, Mar. 15, 2016.

[2] L. I. Albraheem, L. H. Alhudaithy, A. A. Aljaser, M. R. Aldhafian, and G. M. Bahliwah, "Toward designing a Li-Fi-based hierarchical IoT architecture," *IEEE Access*, vol. 6, pp. 40811–40825, 2018.

[3] E. Dutkiewicz, X. Costa-Perez, I. Z. Kovacs, and M. Mueck, "Massive machine-type communications," *IEEE Netw.*, vol. 31, no. 6, pp. 6–7, Nov./Dec. 2017.

[4] M. Shafi *et al.*, "5G: A tutorial overview of standards, trials, challenges, deployment, and practice," *IEEE J. Sel. Areas Commun.*, vol. 35, no. 6, pp. 1201–1221, Jun. 2017.

[5] T. O. Olwal, K. Djouani, and A. M. Kurien, "A survey of resource management toward 5G radio access networks," *IEEE Commun. Surveys Tuts.*, vol. 18, no. 3, pp. 1656–1686, 3rd Quart., 2016.

[6] A. Gupta and R. K. Jha, "A Survey of 5G network: Architecture and emerging technologies," *IEEE Access*, vol. 3, pp. 1206–1232, 2015.

[7] H. Elgala, R. Mesleh, and H. Haas, "An LED model for intensity-modulated optical communication systems," *IEEE Photon. Technol. Lett.*, vol. 22, no. 11, pp. 835–837, Jun. 1, 2010.

[8] H. Burchardt, N. Serafimovski, D. Tsonev, S. Videv, and H. Haas, "VLC: Beyond point-to-point communication," *IEEE Commun. Mag.*, vol. 52, no. 7, pp. 98–105, Jul. 2014.

[9] S. Rajbhandari *et al.*, "Brien, "High-speed integrated visible light communication system: Device constraints and design considerations," *IEEE J. Sel. Areas Commun.*, vol. 33, no. 9, pp. 1750–1757, Sep. 2015.

[10] M. Ayyash *et al.*, "Coexistence of WiFi and LiFi toward 5G: Concepts, opportunities, and challenges," *IEEE Commun. Mag.*, vol. 54, no. 2, pp. 64–71, Feb. 2016.

[11] D. A. Basnayaka and H. Haas, "Design and analysis of a hybrid radio frequency and visible light communication system," *IEEE Trans. Commun.*, vol. 65, no. 10, pp. 4334–4347, Oct. 2017.

[12] H. Haas, "High-speed wireless networkingusing visible light," *SPIE Newsroom*, pp. 1–3, Apr. 2013. doi: 10.1117/2.1201304.004773.

[13] Z. Ghassemlooy, S. Arnon, M. Uysal, Z. Xu, and J. Cheng, "Emerging optical wireless communications-advances and challenges," *IEEE J. Sel. Areas Commun.*, vol. 33, no. 9, pp. 1738–1749, Sep. 2015.

[14] L. Yin and H. Haas, "Coverage analysis of multiuser visible light communication networks," *IEEE Trans. Wireless Commun*, vol. 17, no. 3, pp. 1630–1643, Mar. 2018.

[15] S. S. Bawazir, P. C. Sofotasios, S. Muhaidat, Y. Al-Hammadi, and G. K. Karagiannidis, "Multiple access for visible light communications: Research challenges and future trends," *IEEE Access*, vol. 6, pp. 26167–26174, 2018.

[16] X. Ling, J. Wang, Z. Ding, C. Zhao, and X. Gao, "Efficient OFDMA for LiFi downlink," *J. Lightw. Technol.*, vol. 36, no. 10, pp. 1928–1943, May 15, 2018.

[17] H. Kazemi and H. Haas, "Downlink cooperation with fractional frequency reuse in DCO-OFDMA optical attocell networks," in *Proc. IEEE Int. Conf. Commun. (ICC)*, Kuala Lumpur, Malaysia, May 2016, pp. 1–6.

[18] B. Lin, X. Tang, Z. Ghassemlooy, C. Lin, and Y. Li, "Experimental demonstration of an indoor VLC positioning system based on OFDMA," *IEEE Photon. J.*, vol. 9, no. 2, Apr. 2017, Art. no. 7902209.

[19] H. Marshoud, V. M. Kapinas, G. K. Karagiannidis, and S. Muhaidat, "Non-orthogonal multiple access for visible light communications," *IEEE Photon. Technol. Lett.*, vol. 28, no. 1, pp. 51–54, Jan. 1, 2016.

[20] R. C. Kizilirmak, C. R. Rowell, and M. Uysal, "Non-orthogonal multiple access (NOMA) for indoor visible light communications," in *Proc. 4th Int. Workshop Opt. Wireless Commun. (IWOW)*, Sep. 2015, pp. 98–101.

[21] H. Marshoud, P. C. Sofotasios, S. Muhaidat, G. K. Karagiannidis, and B. S. Sharif, "On the performance of visible light communication systems with non-orthogonal multiple access," *IEEE Trans. Wireless Commun.*, vol. 16, no. 10, pp. 6350–6364, Oct. 2017.

[22] X. Zhang, Q. Gao, C. Gong, and Z. Xu, "User grouping and power allocation for NOMA visible light communication multi-cell networks," *IEEE Commun. Lett*, vol. 21, no. 4, pp. 777–780, Apr. 2017.

[23] M. H. Shoreh, A. Fallahpour, and J. A. Salehi, "Design concepts and performance analysis of multicarrier CDMA for indoor visible light communications," *J. Opt. Commun. Netw.*, vol. 7, no. 6, pp. 554–562, Jun. 2015.

[24] Y.-A. Chen, Y.-T. Chang, Y.-C. Tseng, and W.-T. Chen, "A framework for simultaneous message broadcasting using CDMA-based visible light communications," *IEEE Sensors J.*, vol. 15, no. 12, pp. 6819–6827, Dec. 2015.

[25] H. Marshoud, S. Muhaidat, P. C. Sofotasios, S. Hussain, M. A. Imran, and B. S. Sharif, "Optical non-orthogonal multiple access for visible light communication," *IEEE Wireless Commun.*, vol. 25, no. 2, pp. 82–88, Apr. 2018.

[26] K. Janghel and S. Prakriya, "Performance of adaptive OMA/cooperative-NOMA scheme with user selection," *IEEE Commun. Lett.*, vol. 22, no. 10, pp. 2092–2095, Oct. 2018.

[27] L. Yin, W. O. Popoola, X. Wu, and H. Haas, "Performance evaluation of non-orthogonal multiple access in visible light communication," *IEEE Trans. Commun.*, vol. 64, no. 12, pp. 5162–5175, Dec. 2016.

[28] Z. Chen, Z. Ding, X. Dai, and G. K. Karagiannidis, "On the application of quasi-degradation to MISO-NOMA downlink," *IEEE Trans. Signal Process.*, vol. 64, no. 23, pp. 6174–6189, Dec. 2016.

[29] Y. Mao, B. Clerckx, and V. O. K. Li, "Rate-splitting multiple access for downlink communication systems: Bridging, generalizing, and outperforming SDMA and NOMA," *EURASIP J. Wireless Commun. Netw.*, vol. 2018, no. 1, p. 133, Dec. 2018. doi: 10.1186/s13638-018-1104-7.

[30] Z. Ding *et al.*, "Application of non-orthogonal multiple access in LTE and 5G networks," *IEEE Commun. Mag.*, vol. 55, no. 2, pp. 185–191, Feb. 2017.

[31] Z. Song, Q. Ni, and X. Sun, "Spectrum and energy efficient resource allocation with QoS requirements for hybrid MC-NOMA 5G systems," *IEEE Access*, vol. 6, pp. 37055–37069, Jul. 2018.

[32] C. Chen, D. A. Basnayaka, and H. Haas, "Downlink performance of optical attocell networks," *J. Lightw. Technol.*, vol. 34, no. 1, pp. 137–156, Jan. 1, 2016.

[33] M. B. Rahaim and T. D. C. Little, "Toward practical integration of dual-use VLC within 5G networks," *IEEE Wireless Commun.*, vol. 22, no. 4, pp. 97–103, Aug. 2015.

[34] S. I. Mushfique, P. Palathingal, Y. S. Eroglu, M. Yuksel, I. Guvenc, and N. Pala, "A software-defined multi-element VLC architecture," *IEEE Commun. Mag.*, vol. 56, no. 2, pp. 196–203, Feb. 2018.

[35] Y. Liu, X. Qin, T. Zhang, T. Zhu, X. Chen, and G. Wei, "Decoupled TCP extension for VLC hybrid network," *IEEE J. Opt. Commun. Netw.*, vol. 10, no. 5, pp. 563–572, May 2018.

[36] K. Xu, H.-Y. Yu, Y.-J. Zhu, and Y. Sun, "On the ergodic channel capacity for indoor visible light communication systems," *IEEE Access*, vol. 5, pp. 833–841, 2017.

[37] H. Marshoud, P. C. Sofotasios, S. Muhaidat, B. S. Sharif, and G. K. Karagiannidis, "Optical adaptive precoding for visible light communications," *IEEE Access*, vol. 6, pp. 22121–22130, 2018.

[38] M. S. Demir, S. M. Sait, and M. Uysal, "Unified resource allocation and mobility management technique using particle swarm optimization for VLC networks," *IEEE Photon. J.*, vol. 10, no. 6, Dec. 2018, Art. no. 7908809.

[39] M. F. Sanya, L. Djogbe, A. Vianou, and C. Aupetit-Berthelemot, "DC-biased optical OFDM for IM/DD passive optical network systems," *J. Opt. Commun. Netw.*, vol. 7, no. 4, pp. 205–214, Apr. 2015.

[40] M. Zhang and Z. Zhang, "An optimum DC-biasing for DCO-OFDM system," *IEEE Commun. Lett.*, vol. 18, no. 8, pp. 1351–1354, Aug. 2014.

[41] S. Dimitrov and H. Haas, "Information rate of OFDM-based optical wireless communication systems with nonlinear distortion," *J. Lightw. Technol.*, vol. 31, no. 6, pp. 918–929, Mar. 15, 2013.

[42] Z. Wei, J. Guo, and J. Yuan, "Fairness comparison of uplink NOMA and OMA," in *Proc. IEEE Veh. Technol. Conf. (VTC Spring)*, Jun. 2017, pp. 1–6.

[43] A. S. Marcano and H. L. Christiansen, "A novel method for improving the capacity in 5G mobile networks combining NOMA and OMA," in *Proc. IEEE 85th Veh. Technol. Conf. (VTC Spring)*, Jun. 2017, pp. 1–5.

[44] A. Ishizaka and P. Nemery, *Multi-Criteria Decision Analysis: Methods and Software*. Hoboken, NJ, USA: Wiley, 2013.

[45] Z. Zhang, H. Sun, and R. Q. Hu, "Downlink and uplink non-orthogonal multiple access in a dense wireless network," *IEEE J. Sel. Areas Commun.*, vol. 35, no. 12, pp. 2771–2784, Dec. 2017.

HAMADA ALSHAER (M'02–SM'13) received the Ph.D. degree in computer engineering and telecommunications from Pierre et Marie Curie University, France, in 2005. He is currently involved in software defined wireless networking, security, and mobile networks virtualization research development with the LiFi Research and Development Centre, School of Engineering, The University of Edinburgh, U.K. He has researched for more than 14 years with British Telecom, Etisalat, INRIA, France, and Leads University, in academic and industrial research development. He has authored more than 50 papers in various research topics in electrical and computer engineering including information technology and systems and authored a book *Demanding Traffic Control and Management in Next Generation Networks: QoS Analysis, Network Simulation, Performance Modelling* (LAP LAMBERT Academic Publishing, 2009). His research interests include cross-layer design for vehicular networks, software-defined wireless networking, wireless networks virtualization, mobile communications security, optical communications and networking, wireless sensor networks, and intelligent transportation. He was a recipient of the 2009 Royal Academy of Engineering Travel Award, and scholarships from UNRWA, French government, and Pierre et Marie Curie University for academic distinctions. He has served on the technical program committee of various IEEE conferences, including the IEEE Intelligent Vehicles Symposium, Vehicular Technology Conference, GLOBECOM, ICC, and WCNC, and chaired some of their sessions. He is a regular reviewer for research grants submitted for prestigious funding bodies in Europe, Asia, and Middle East.

HARALD HAAS (S'98–A'00–M'03–SM'16–F'17) is currently the Chair of mobile communications with The University of Edinburgh and also the Principal, a Co-Founder, and a Chief Scientific Officer of pureLiFi Ltd. He is also the Director of the LiFi Research and Development Center (LRDC), The University of Edinburgh. He first introduced and coined spatial modulation and LiFi, in 2006 and 2011, respectively. LiFi was listed among the 50 best inventions in *TIME Magazine* 2011. He was an Invited Speaker at TED Global 2011, and his talk: Wireless Data from Every Light Bulb has been watched online more than 2.6 million times. He gave a second TED Global lecture, in 2015 on the use of solar cells doubling as LiFi data detectors and energy harvesters. This has been viewed online more than 2.4 million times. He holds 47 patents and has more than 30 pending patent applications. He has published more than 450 conference and journal papers including a paper in Science. He was elected a Fellow of the Royal Society of Edinburgh (RSE), in 2017. In 2018, he received an extension of his EPSRC Established Career Fellowship. In 2012, he was a recipient of the prestigious Established Career Fellowship from the Engineering and Physical Sciences Research Council (EPSRC), U.K. He was a recipient of the Tam Dalyell Prize 2013 awarded by The University of Edinburgh for excellence in engaging the public with science. He has been on the Thomson Reuters list of Highly Cited Researchers, in 2017 and 2018. In 2017, he received a Royal Society Wolfson Research Merit Award, and was elevated to IEEE Fellow. He has delivered 50 keynotes talks at international conferences and workshops. In 2014, he was selected by EPSRC as one of ten Recognising Inspirational Scientists and Engineers (RISE) Leaders in U.K. In 2016, he received the outstanding achievement award from the International Solid State Lighting Alliance.

HANAA ABUMARSHOUD received the M.Sc. and Ph.D. degrees in electrical and computer engineering from Khalifa University, United Arab Emirates, in 2013 and 2017, respectively. She is currently a Research Associate with the LiFi Research and Development Centre, Institute for Digital Communications (IDCOM), The University of Edinburgh. Her current research interest includes the application of information theory and signal processing techniques in optical communications with a particular focus on visible light communication and LiFi systems.

• • •